nature communications

Article

https://doi.org/10.1038/s41467-024-55475-5

Neuronal segmentation in cephalopod arms

Received: 27 June 2024

Accepted: 9 December 2024

Published online: 15 January 2025

Check for updates

Cassady S. Olson [1] ✉, Natalie Grace Schulz [2] & Clifton W. Ragsdale [2,3]

Prehensile arms are among the most remarkable features of the octopus, but little is known about the neural circuitry controlling arm movements. Here, we report on the cellular and molecular organization of the arm nervous system, focusing on its massive axial nerve cords (ANCs). We found that the ANC is segmented. In transverse cross sections, the ANC cell body layer wraps around the neuropil with no apparent segregation of sensory and motor neurons. In longitudinal sections, however, ANC neurons form segments, setting up a modular organization to the adjoining neuropil. ANC nerves exit in the septa between segments, and for each sucker, form a spatial topographic map ("suckerotopy"). A strong link between ANC segmentation and flexible sucker-laden arms is confirmed by comparative study of squid arms and tentacles. These ANC modules offer a template for modeling the motor control of soft tissues and provide a compelling example of nervous system segmentation in molluscs.

The octopus has a motor control challenge of enormous complexity[1,2]. Each of its eight arms is a muscular hydrostat, a soft-bodied structure that lacks a rigid skeleton and moves with near infinite degrees of freedom[3,4]. Moreover, the arms are packed with hundreds of chemotactile suckers which can change shape independently[5,6]. Even with this complexity, octopuses control behaviors effectively along the length of a single arm, across all eight arms and between suckers (Supplementary Movie 1)[7–9]. The neural circuits underlying these behaviors have been unexplored with modern molecular and cellular methods.

Embedded in the octopus arm is a massive nervous system, with more neurons found distributed across the eight arms than in the brain[10,11]. Most prominent is an axial nerve cord (ANC) running down the center of every arm (Fig. 1a, Supplementary Fig. 1a)[2,12]. Peripheral to the ANC, there are four smaller intramuscular nerve cords (IMNCs), and a sucker ganglion (SG) for every sucker (Fig. 1a, Supplementary Fig. 1a). In the ANC, and following the characteristic invertebrate pattern, neuronal cell bodies are localized to a cell body layer (CBL) wrapping around neuropil (NP). Down the long axis of the arm, the ANC is a medullary cord[13] that snakes back and forth, with every bend in the ANC forming an ANC enlargement that overlies a sucker[14] (these ANC enlargements are themselves sometimes referred to as ganglia[11,15,16], see Supplementary Fig. 1g, h). In transverse sections on the sucker, or oral, side of the ANC, the CBL forms a horseshoe around the NP (Fig. 1b, Supplementary Fig. 1b). On the aboral side, or away from the suckers, there is a massive cerebro-brachial tract (CBT) connecting the arms and the brain[12,17] (Fig. 1b, Supplementary Fig. 1b). The CBL itself can be divided into an aboral, or brachial, territory that is dedicated to the sensorimotor control of the arm, and an oral, or sucker, territory for the sensorimotor control of the suckers[18] (Supplementary Fig. 1g, h). Beyond this classical segregation, further neural divisions within the ANC and in the ANC nerve trajectories for the brachial musculature and the suckers are unknown.

In this study, we investigated the structure of the ANC and its nerves in *Octopus bimaculoides* using modern molecular and cellular techniques. We found that the ANC is segmented, forming columns of neuronal cell bodies. These neuronal segments underlie a modular organization to the ANC neuropil: neuronal cell bodies within each segment send the bulk of their processes directly into the adjoining neuropil, with some reaching the contralateral side. The septa between each segment are neuron-poor but contain nerve exits, vasculature and abundant collagen. Nerves exiting from neighboring septa differ in their fiber trajectories indicating that multiple adjoining segments must cooperate to innervate the arm musculature fully. The nerves for each sucker also exit through septa, radially tiling the sucker to create a spatial topographic map in the ANC. In the squid *Doryteuthis pealeii*, the arms and the sucker-rich club of the tentacles have segments, but the sucker-poor stalk of the tentacles does not, suggesting a strong link between segmentation and flexible sucker-laden arms. Our findings in

[1]Committee on Computational Neuroscience, The University of Chicago, Chicago, IL, USA. [2]Committee on Development, Regeneration and Stem Cell Biology, The University of Chicago, Chicago, IL, USA. [3]Department of Neurobiology, The University of Chicago, Chicago, IL, USA.
✉e-mail: olsoncs@uchicago.edu

https://doi.org/10.1038/s41467-024-55475-5

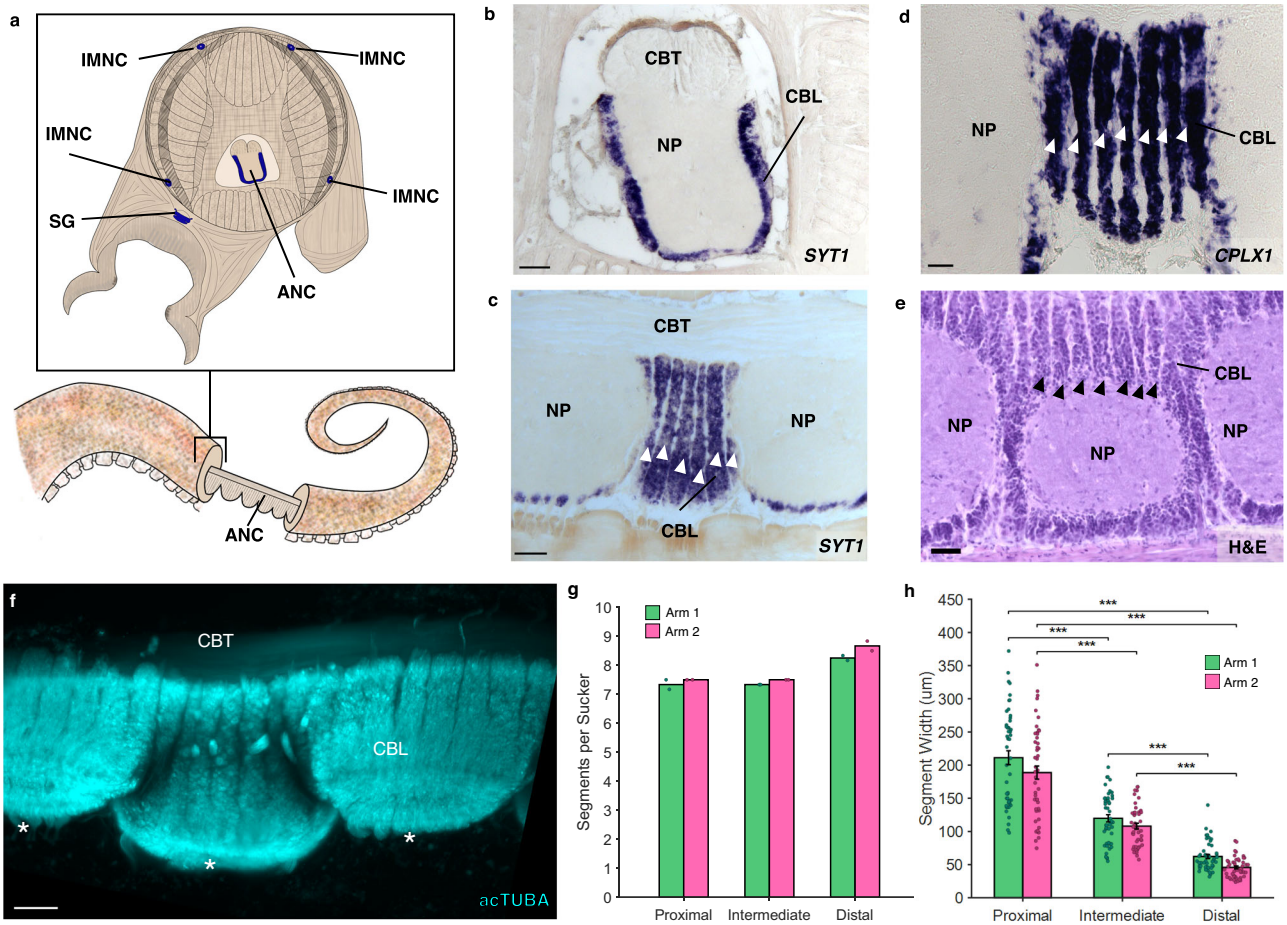

Fig. 1 | The axial nerve cord (ANC) is segmented. a Transverse diagram of *O. bimaculoides* arm with the location of neuronal cell bodies outlined in blue. **b** In situ hybridization (ISH) for synaptotagmin 1 (*SYT1*) in a transverse section of the ANC. Representative sample from 7 explants. Scale bar: 100 µm. **c**–**e** Longitudinal sections through the ANC demonstrating segmentation in the cell body layer with (**c**) ISH for *SYT1*, representative sample from 21 explants. Scale bar: 100 µm, **d** ISH for complexin (*CPLX1*), representative sample from 7 explants and (**e**) hematoxylin and eosin (H&E), representative sample from 6 explants, scale bars: 50 µm. Arrowheads point to individual segments. **f** Whole mount immunostaining with acetylated alpha-tubulin (acTUBA) of a dissected ANC. Segmentation pattern is continuous as the ANC oscillates from sucker to sucker. Representative sample from 7 explants. * denotes individual suckers. Scale bar: 100 µm. **g**, **h** Quantification of segmentation down the proximal-distal axis. Arm 1 (green) was stained with acTUBA and arm 2 (pink), with H&E. **g** The number of segments per sucker is maintained along the proximal-distal axis ($n = 2$ per condition, average Arm 1 = 7.64; average Arm 2 = 7.88). **h** Segment width decreases down the proximal-distal axis. Data represent mean +/- sem ($n = 48$ per condition). $P < 0.001$, 2-way ANOVA, with post hoc Tukey's test. CBL, cell body layer; CBT, cerebrobrachial tract; IMNC, intramuscular nerve cord; NP, neuropil; SG, sucker ganglion.

squid and octopus constitute a clear demonstration of segmental organization in a mollusc.

Results

Segmentation in the ANC

We found an unexpected neuronal organization in the ANC along the longitudinal axis of the arm: neuronal cell bodies are constrained to segmental columns separated by septa (Fig. 1c, d, e). These segments encompass the full aboral to oral extent of the cell body layer, involving both the brachial and sucker territories (Supplementary Fig. 1g, h). The segmentation pattern persists as the ANC weaves from sucker to sucker (Fig. 1f, Supplementary Fig. 1f, g, h). The arm tapers and suckers become smaller along the proximal-distal axis of the arm, as do the widths of the segments (Fig. 1h, Supplementary Fig. 1d, e). The consequence is the number of segments per sucker remains constant (average: ~7.5; Fig. 1g).

We investigated the septa between segments. The space between the CBL segments is enriched with connective tissue, labeled by Picrosirius Red staining (Fig. 2a). Connective tissue pads the length of the septa, and sometimes lines the interface between the CBL and NP (Supplementary Fig. 2f). Vasculature also lies in the septa. Most prominent is F-actin-positive vasculature that travels along the inner border of the CBL and the NP, strictly following the segmental boundaries (Fig. 2b, Supplementary Fig. 2e). To confirm that this F-actin labeling identifies blood vessels[19], we flooded the vascular system with dextran-TRITC. We found an overlap of the vasculature labeled with the dextran and by the F-actin staining (Fig. 2c, d, Supplementary Fig. 2b, c, d). Thus, as with other segmental systems, such as in insect developmental compartments or vertebrate somites[20–22], multiple tissue types form in a segmental pattern along the ANC.

Relationship to sensorimotor circuits

Nerve fibers depart at discrete points along the oral to aboral extent of the ANC, utilizing the septa as exit points (Fig. 2e, f, g). Physiological and classic neuroanatomical studies have shown that these nerves carry both sensory and motor information[23–25]. Given this result, we used molecular markers to ask whether there might be a segregation of sensory and motor territories within the CBL itself. Markers of motor neurons (*NKX6, MNX, LHX3*) are largely restricted to the lateral sides of the CBL (Supplementary Fig. 3a, b, c, d). Markers of primary sensory neurons (*DRGX, PIEZO*) are also found distributed throughout this

https://doi.org/10.1038/s41467-024-55475-5

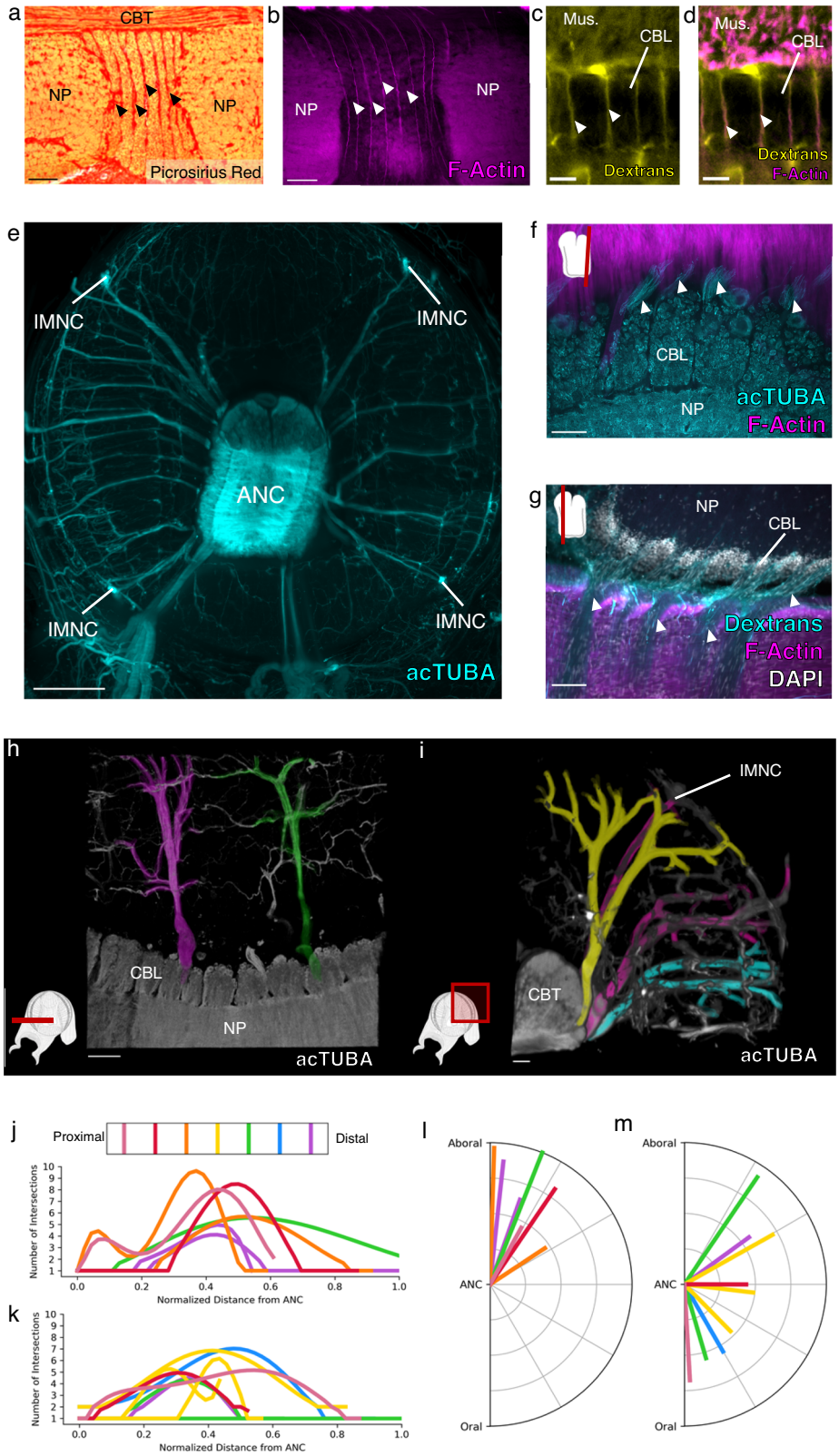

territory (Supplementary Fig. 3e, f, g). These results indicate that, unlike vertebrate spinal cord[26], there is not a clear spatial separation of sensory and motor neurons within the ANC.

Nerves exiting the ANC can be divided into the oral nerves, which innervate the sucker, and aboral and central nerves, which together innervate the brachial musculature[12,15] (Fig. 2f, g, Supplementary Fig. 4a). We asked how the ANC nerve fibers relate to the segmentation within the ANC by examining the innervation patterns of the aboral and central nerves targeting the brachial muscles. One possibility is that the same pattern of nerves is found between every segment. If this were the case, each CBL segment would reflect the same sensorimotor unit, simply spatially shifted down the longitudinal axis of the arm (See Supplementary Fig. 5b). We studied brachial nerve fiber trajectories with whole mount immunohistochemistry for acetylated alpha-tubulin

Fig. 2 | Organization of the septa and the innervation patterns of the brachial musculature. a Picrosirius Red stain of an axial nerve cord (ANC) longitudinal section. Red denotes the presence of collagen. Arrowheads point to collagen-rich septa. Representative sample from 3 explants. Scale bar: 100 µm. **b** F-actin (magenta) labeled by phalloidin is localized to the septa, indicated by arrowheads. Representative sample from 16 explants. Scale bar: 100 µm. **c** Trans-vascular dextran labeling demonstrates vasculature (yellow) in the septa. Representative sample from 25 explants. Scale bar: 20 µm. **d** Dextran labeling colocalizes with F-actin staining (magenta). Representative sample from 25 explants. Arrowheads point to septa. Scale bar: 20 µm. **e** Maximum projection of acetylated alpha-tubulin (acTUBA) whole mount immunostaining of a transverse slice. Nerve fibers exit the ANC at discrete locations. Representative sample from 20 explants. Scale bar: 500 µm. **f**, **g** Longitudinal ANC sections of the brachial nerve exits in the septa, indicated by arrowheads. **f** acTUBA nerve labeling (cyan), representative sample from 11 explants. **g** Experimental dextran tracing of oral nerves. Injection site in central NP. Representative sample from 8 explants. Scale bars: 100 µm. **h**–**m** Brachial nerves exiting from neighboring septa have different targets. **h** Maximum projection of a horizontal whole mount stained with acTUBA. Two nerves (false colored in magenta and green) innervating similar territories of muscle are separated by multiple segments. Representative sample from 10 explants. (**i**) Maximum projection of a transverse whole mount stained with acTUBA. Three nerves (false colored with yellow, magenta and cyan) exiting from neighboring septa target different brachial territories. Representative sample from 19 explants. Scale bars: 100 µm. (**j**–**k**) Branching profiles of nerves across multiple septa were characterized by Sholl analysis. Profiles differ from septum to septum. **j** Aboral nerves. **k** Central nerves. **l**, **m** Nerve fiber average trajectories vary across septa. **l** Aboral nerves. **m** Central nerves. Mus., brachial musculature.

(acTUBA) and in dextran tracer experiments. The average exit trajectory and branching profile, calculated with Sholl analysis, were found to compare nerves exiting between adjoining and more distant septa (Supplementary Fig. 4). For both the central and aboral nerves, nerves exiting between adjoining septa exhibit different branching profiles and exit with different average trajectories (Fig. 2i–m). Nerves with similar branching profiles and exit trajectories are separated by multiple septa (Fig. 2h, Supplementary Fig. 4). We found, however, that nerve fibers across multiple septa collectively provide full coverage of the brachial musculature (Supplementary Fig. 5). Instead of each segment reflecting identical sensorimotor units, this innervation pattern predicts that adjoining segments collaborate in organizing the brachial muscle activation patterns. Alternating innervation patterns have been documented in other segmented systems, such as that of the rhombomeres in the developing vertebrate hindbrain[27].

We next interrogated the structure of the NP in the brachial territory of the ANC. Neuronal cell bodies send their projections directly into the NP adjacent to their segments, effectively partitioning the NP (Fig. 3a, Supplementary Fig. 6b). Some of these projections extend across the midline, predicting crosstalk from segments on one side of the ANC to those on the other (Fig. 3a, Supplementary Fig. 6c). In addition, as aboral and central nerve fibers enter the ANC, they branch into segments both proximal and distal to the septum of entry, leading to an overlap of the projections in the NP of nerve fibers from neighboring septa (Fig. 3b). Collectively, this circuit structure provides the neural substrate for integration of multiple segments in the control of the brachial musculature (Fig. 3c).

The sucker is the second major target of the ANC, and we examined the relationship of oral roots innervating the sucker to the ANC segmentation. The expansion of the oral ANC opposite to each sucker was targeted for axon tracing, and, as the example illustrated in Fig. 3g demonstrates, the oral nerves arising from each enlargement target a single sucker. This result was confirmed with acTUBA immunostaining (Supplementary Fig. 6j). After exiting the ANC in the septa, the oral roots radially tile the sucker, reaching both the muscles of the sucker and the chemotactile sensory epithelium on the rim of the sucker (Fig. 3h, Supplementary Fig. 6k, l, m). Nerve fibers from neighboring septa target adjoining territories along the sucker (Supplementary Fig. 6l). This arrangement establishes a spatial topography for the sucker in the ANC ("suckerotopy") based on nerve exits.

We next followed the oral nerves into the ANC neuropil, where they maintain their spatial segregation, establishing an internal ANC suckerotopy (Fig. 3d). As demonstrated by DiI crystal placement within a sucker, the oral nerves enter on both sides of the ANC (Supplementary Fig. 7g). Nerve fibers first branch locally, demonstrating short-range projections to ipsilateral nerves entering in adjoining septa (Fig. 3d, Supplementary Fig. 6h, i). As the oral roots progress further into the NP, they show projections to NP on the contralateral side (Supplementary Fig. 6g, h). Lastly, the oral roots branch to engage in mid-range projections to the ANC segments of adjoining suckers (Fig. 3d, e, f). This circuitry demonstrates pathways for both intra-sucker and inter-sucker communication.

Because the oral nerves for a single sucker enter on both sides of the ANC, nerves arising from one side of the ANC connect to the internal side of the sucker (InS) and nerves arising from the other side connect to the external side of the sucker (ExS) (Supplementary Fig. 7a, b). We discovered that segments are expanded on the ExS of the ANC (ExA) as compared with the InA (Supplementary Fig. 7d, e). Since segments correspond to spatial territories along the sucker, this arrangement suggests that more neural territory is dedicated to the ExS. Accordingly, we found the oral roots corresponding to the ExS cover ~65% of the sucker, whereas the roots issued to the InS cover the remaining 35% (Fig. 3i, Supplementary Fig. 7h–j). The sucker sensory epithelium is evenly innervated, with no obvious bias to the ExS side over the InS side (Fig. 3h, Supplementary Fig. 6m). Consequently, the asymmetry in segment width is accounted for by an asymmetry in the amount of spatial territory covered, indicating an anisotropic sensorymotor topographic map for a sucker in the ANC.

Comparative analysis

We carried out a comparative analysis to clarify the relationship between ANC segmentation and function by examining the organization of the ANC of the longfin inshore squid, *Doryteuthis pealeii*. Squids, which diverged from octopuses 270 million years ago, have two tentacles in addition to eight sucker-lined arms[28] (Fig. 4a, e, i). Like octopuses, these limbs are muscular hydrostats, yet they differ in gross morphology and function[29,30]. Where *O. bimaculoides* is benthic, with arms suited for exploration and movement on the seafloor, *D. pealeii* is a pelagic animal and primarily uses its arms and tentacles for prey capture in open water[8]. The tentacle stalks, which are devoid of suckers, rapidly elongate to grab prey with tentacle clubs, the sucker-rich ends of the tentacles. The arms enclose the prey in a coordinated movement as the prey is brought back to the mouth. Morphological differences between squid arm and tentacle muscle composition underlying this functional difference have been described[30,31].

In the arms, tentacle stalks and clubs of *D. pealeii*, there is an ANC mediating sensorimotor control (Fig. 4b, f, j). The ANC in the squid has a notably different arrangement from that of octopus, however. The CBL is restricted to the ANC lateral edges, with large longitudinally running fiber-tracts both orally and aborally (Fig. 4b, f, j). In the tentacle, the CBL thins along the stalk but expands in the sucker-rich club (Fig. 4f, j). We used gene expression and phalloidin staining to look for segmentation in the squid CBL. The CBL in the arm of the squid is segmented, with ~4.5 segments per sucker (Fig. 4c, d). As in *O. bimaculoides*, F-actin is localized to the ANC septa (Supplementary Fig. 8a). In the tentacle stalk, however, CBL segments as identified by synaptotagmin 1 (*SYT1*) gene expression are at best indistinct, and although F-actin marks regularly spaced vasculature, these are not in the CBL (Fig. 4g, h, Supplementary Fig. 8b). In the sucker-rich tentacle club, by contrast, CBL segments marked by *SYT1* and F-actin within the CBL are

https://doi.org/10.1038/s41467-024-55475-5

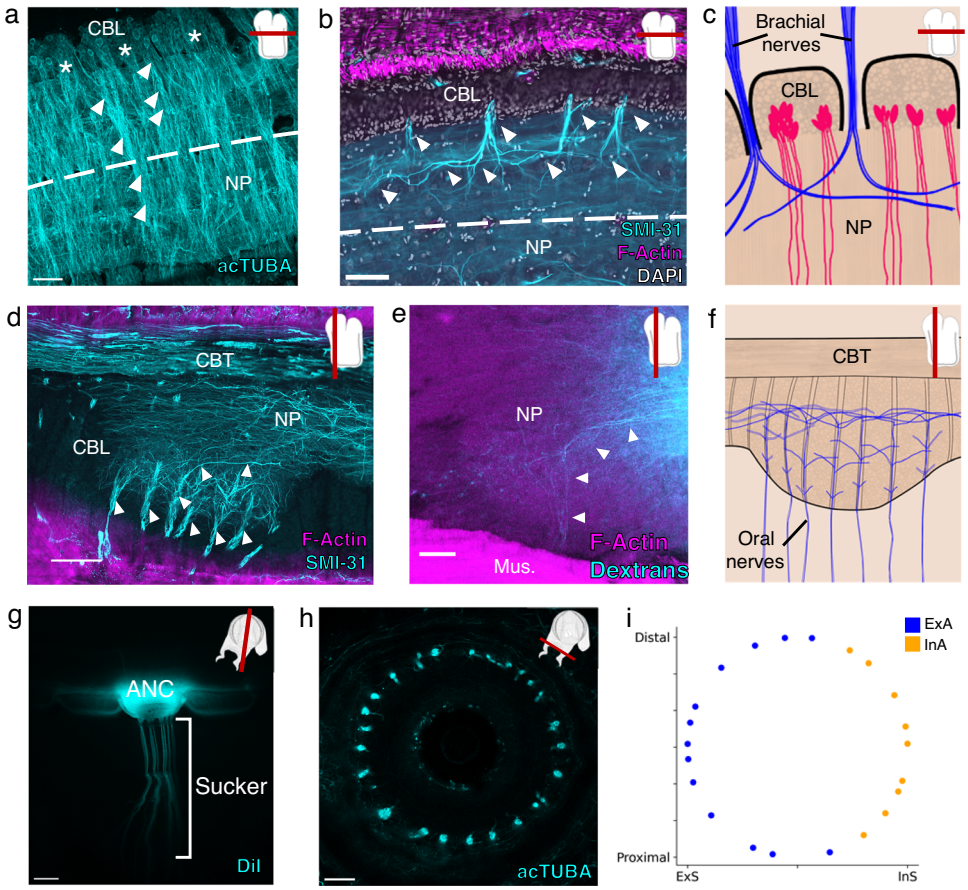

Fig. 3 | Organization of the neuropil (np) and the innervation patterns of the suckers. a–c Aboral, or brachial, NP. **a** Maximum projection of a horizontal acTUBA wholemount (cyan), showing that the bulk of each cell body segment extends its processes into the NP of the segment. Some processes cross the midline (dashed line). * denotes individual segments. Arrowheads point to cell body projections. Representative sample from 12 explants. **b** Horizontal section immunostained with SMI-31 (cyan), phalloidin (magenta) and DAPI (gray). SMI-31-rich subpopulation of nerve fibers (cyan, denoted with arrowheads) branch proximally and distally upon entering the ANC. Representative sample from 13 explants. **c** Diagram of a horizontal section through the brachial NP. Nerve fibers (blue) pool across neurons (magenta) arranged in segments. Scale bars: 100 µm. **d–f** Oral, or sucker, NP. **d** Longitudinal ANC section stained with SMI-31 (cyan) and phalloidin (magenta). NP fibers (cyan) collect into internal fascicles before exiting as oral nerves, indicated with arrowheads. Representative sample from 13 explants. **e** Longitudinal section of NP dextran tracer-deposit (cyan) demonstrating NP fibers forming a fascicle, pointed to by arrowheads. Representative sample from 6 explants. **f** Diagram of NP fibers in the longitudinal plane. From oral to aboral, oral nerves enter the ANC, first showing local branching, then more extensive branching. Scale bars: 100 µm. **g–i** Oral ANC nerves distributed around a sucker. **g** Longitudinal whole mount. DiI crystal (cyan) placed in a single ANC sucker enlargement targets a single sucker. Representative sample from 4 explants. Scale bar: 500 µm. **h** Horizontal acTUBA-stained section through a sucker demonstrates radially symmetric decoration. Representative sample from 34 explants. Scale bar: 100 µm. **i** Distribution of oral nerve fiber tips around a sucker. Nerves from the external ANC side (ExA) are tagged in blue; nerves from the internal side (InA), in orange. Data from a transversely imaged whole mount stained with acTUBA. The ExA covers 68% of the sucker; the InA, 32%.

readily identified (Fig. 4k, l, Supplementary Fig. 8c). This comparative anatomy suggests a strong link between ANC segmentation and flexible cephalopod arms lined with suckers.

Discussion

The cephalopod arm is a highly redundant structure, with both suckers and the pattern of brachial musculature repeated down its length[1,2]. A parcellation of the ANC into segments is a natural way to relegate motor control of a continuous limb with such a reiterated structure. In fact, many computational models and soft robots inspired by octopus arms divide the arm into repeated segments in their construction or control algorithms[32–35]. Our results, however, demonstrate additional complexities. For the brachial musculature, different sets of nerves exit from adjoining septa, while still providing coverage of the musculature. Instead of a single segment representing the full cylinder of brachial musculature, as is the case in many models, adjoining segments coordinate in parsing control for the muscles. This circuit structure could more effectively smooth continuous movements along the length of the arm, as well as isolate contractions to localized territories in the brachial musculature. The brachial musculature also contains peripheral nervous system elements, such as the intramuscular nerve cords, to which the nerves connect. These peripheral mechanisms could serve as additional pathways for communication between nerves, further linking nerves that are separated by multiple segments.

The ANC contains enlargements corresponding to the location of the suckers[12,14]. The neuronal segments described here further subdivide these swellings into multiple modules. Classic studies have proposed that much of the sensorimotor processing in suckers occurs within the epithelium or in the sucker ganglion, and that by the time the information reaches the ANC, it has been highly downsampled[36,37]. Our investigation of nerve fiber connections illustrates that, at the least, spatial information is preserved within the ANC, creating a suckerotopy. Combined with the projections that interconnect suckers, such a neural architecture would support many behaviors seen in suckers, from passing objects along the suckers to the anisotropic

https://doi.org/10.1038/s41467-024-55475-5

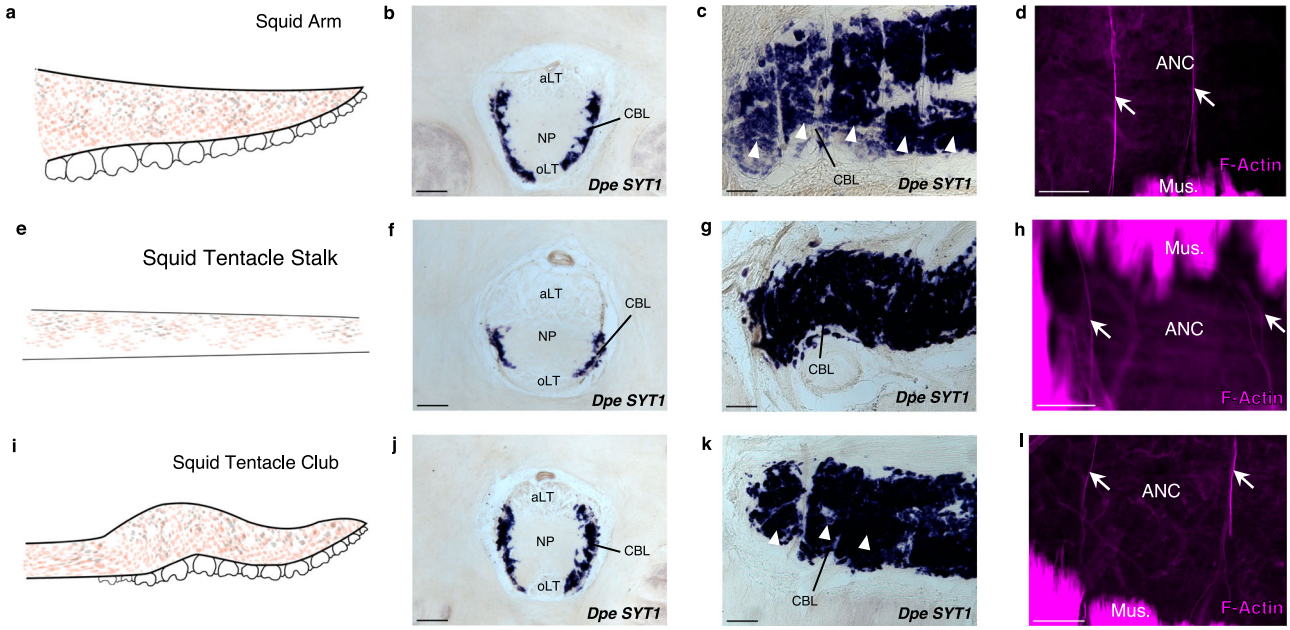

Fig. 4 | Segmentation is a shared feature of flexible, sucker-laden cephalopod appendages. a–d The axial nerve cord (ANC) of the *D. pealeii* arm is segmented. **a** Cartoon depiction of *D. pealeii* arm, which has suckers. **b** ISH for *Dpe SYT1* of an ANC transverse section labeling the cell body layer (CBL). Representative sample from 3 explants. **c** ISH for *Dpe SYT1* of an arm longitudinal section demonstrates CBL segmentation. Representative sample from 5 explants. **d** F-actin (magenta) marks vasculature in the arm ANC septa. Representative sample from 3 explants. **e–h**, The ANC of the tentacle stalk lacks CBL segmentation. **e** Cartoon depiction of *D. pealeii* tentacle stalk, which is devoid of suckers. **f** Transverse ISH section for *Dpe SYT1* demonstrates a clear, although reduced, tentacle CBL. Representative sample from 3 explants. **g** *Dpe SYT1* ISH of a longitudinal ANC section does not show CBL segmentation in the tentacle stalk. Representative sample from 3 explants. **h** F-actin (magenta) demonstrates a regularly arranged vasculature in the tentacle stalk, but these blood vessels do not lie within the CBL. Representative sample from 4 explants. **i–l** The ANC in the tentacle club has segments. **i** Cartoon depiction of *D. pealeii* tentacle club, which is located at the end of the stalk and has suckers. **j** Transverse ISH section for *Dpe SYT1* in the tentacle club ANC demonstrates the CBL. Representative sample from 2 explants. **k** Longitudinal *Dpe SYT1* section of the tentacle club CBL shows segmentation. Representative sample from 2 explants. **l** F-actin (magenta) identifies regularly spaced vasculature in the tentacle club septa. Representative sample from 2 explants. White arrowheads in (**c, k**) point to CBL segments. White arrows in (**d, h, l**) indicate phalloidin-labeled blood vessels. aLT, aboral longitudinal tract; oLT, oral longitudinal tract. Scale bars: 100 µm.

detection of chemical cues[5,38–40]. In particular, deformation of individual suckers has been thought to underlie shape discrimination[41]. This spatial mapping could be the basis for ring attractor computations by the axial nerve cord to guide sucker movements in response to sensory cues. Such a mechanism has been described for spatial navigation in the central complex of *Drosophila*[42], and recently it has been suggested in biophysical models of directed movements by octopus arms[43].

Molluscs are a diverse phylum, and cephalopods in particular exhibit many derived morphologies. Our comparative analysis emphasizes that this segmentation is a derived feature in flexible, sucker-laden arms. Segments are present in the arm and tentacle club in *D. pealeii*, yet they are indistinct in the stalk, which is devoid of suckers. Interestingly, there are fewer segments per sucker in the arm of *D. pealeii* compared with that of *O. bimaculoides*. Differences in ecological niche and behavioral repertoire, including prey hunting strategies, could drive this variation[8,40].

There has long been a vigorous discussion in the evolutionary and developmental biology fields about whether segmentation is an ancestral feature of bilateral animals[44]. In molluscs, segmentation has been proposed as a shared feature of polyplacophorans (chitons) and monoplacophorans[45,46], but the evolutionary interpretations of this similarity have been hotly contested[47–50] and, at the least, have not been proposed to encompass the nervous system. A second view of segmentation is that it represents an adaptation useful for generating vermiform movements[46,51]. Our findings provide a clear example of the second view, that of derived segmentation linked to the control of the motor patterns characteristic of soft-bodied cephalopod (coleoid) arms. This segmentation shares many similarities to segmentation described in other systems: multiple tissue types, reiterated patterning along a longitudinal axis, and utilization for sensorimotor control circuitry[20–22,27]. Whether in development ANC segment generation shares any similarities to segmental patterning mechanisms in other animals[44] will be important to investigate in future studies. At the adult functional and structural levels, however, the coleoid segmentation appears to reflect one role, that of setting up recurring neuronal modules dedicated to the control of muscles and suckers which are themselves reiterated down the length of the arms.

Methods

These cephalopod experiments were performed in compliance with the EU Directive 2010/63/EU guidelines on cephalopod use, the University of Chicago Animal Resources Center and the MBL and UChicago Institutional Animal Care and Use Committees[52,53].

Animals

Wild caught adult *Octopus bimaculoides* of both sexes and at least six months of age were purchased from Aquatic Research Consultants, a field-collection venture operated by Dr. Chuck Winkler, San Pedro, CA. Animals were individually housed in 20-gallon saltwater tanks equipped with a carbon particle filter, aquarium bubbler, and an UV light. Animals were fed daily with fiddler crabs. The artificial seawater (ASW) was prepared in deionized water from pharmaceutically pure sea salt (33 g/liter; Tropic Marin "classic", Wartenberg, Germany). Sex was recorded in sexually mature animals, but not studied. Adults were deeply anesthetized in 4% ethanol/ASW (EtOH/ASW, $n = 17$) and transorbitally perfused with 4% paraformaldehyde/phosphate-buffered saline solution (PFA/PBS, pH 7.4) delivered via a peristaltic pump (Cole Parmer Masterflex) through a 21½ gauge needle (Becton Dickinson).

The left and right white bodies, a hematopoietic tissue, were targeted alternately and iteratively throughout the procedure. Arms were dissected and stored in 4% PFA/PBS overnight at 4 °C. Specimens were then either cut into 2–4 cm pieces for immediate processing or stored in diethyl pyrocarbonate (DEPC) treated-PBS at 4 °C.

Wild caught adult *Doryteuthis pealeii* ($n = 3$) were obtained from the Marine Biological Laboratory, Woods Hole, MA. Animals were kept in circulating, filtered containment tanks for several days before being deeply anesthetized in 7.5% $MgCl_2$/ASW and dissected. Arm crowns were immersion fixed in 4% PFA/PBS. Arms and tentacles were dissected and cut into 2–4 cm pieces for further processing.

Tissue Processing

For sections, arm explants were incubated in 30% sucrose/4%PFA/PBS at 4 °C for three to five days until saturated, rinsed with 30% sucrose/PBS, and infiltrated with 10% gelatin/30% sucrose/PBS for 1 h at 50 °C. Tissue was embedded in 10% gelatin/30% sucrose/PBS and post-fixed in 30% sucrose/4%PFA/PBS before storage at −80 °C. Gelatin-embedded serial arm sections were cut at 28–50-μm thickness on a freezing microtome (Leica SM2000R) and collected in DEPC-PBS. Sections were mounted and dried on charged, hydrophilic glass slides (TruBond380, Newcomer Supply, Middleton, WI). Slides were stored at −80 °C until further processing.

Immunohistochemistry

Neuronal processes in octopus arm were labeled with mouse monoclonal antibody 6–11B-1 (1:500 dilution of ascites fluid; Sigma-Aldrich, Cat#: T6793) and mouse monoclonal antibody SMI-31 (1:500 dilution; BioLegend, Cat# 801601). Clone 6–11B-1 was isolated following immunization with sea urchin sperm flagella protein preparations[54]. It recognizes an acetylated α-tubulin (acTUBA) epitope found broadly but not universally across microtubules and has been extensively employed to identify axon tracts in vertebrate and invertebrate nervous systems[55–58]. Clone SMI-31 reacts with a phosphorylated epitope of neurofilament in mammals and neurofilament 220 in squid[59–61].The secondary Alexa Fluor® 488 AffiniPure Goat Anti-Mouse IgG (Cat#: 115-545-003) and Cy™3 AffiniPure Donkey Anti-Mouse IgG (Cat#: 715-165-151) were purchased from Jackson ImmunoResearch (West Grove, PA) and employed at 1:500 dilutions.

For section immunohistochemistry, slides were rinsed 3 × 10 min (3 times for 10 min each) in DEPC-PBS containing 1% tween 20 (PBST) and incubated for 30 min in a proteinase K solution (Sigma-Aldrich, Cat#: 03115828001; 19.4 μg proteinase K per milliliter of PBST). Slides were post-fixed with 4% PFA/PBS, washed 3 × 30 min in PBST, blocked in 10% goat serum/PBST (Fisher Scientific, Cat#: 16210072) for 1 h and incubated in primary antibody diluted in 1% goat serum/PBST for four days at 4 °C. After 3 × 30 min PBST washes, sections were incubated for two days at 4 °C with secondary antibody along with 0.01 mg/ml 4′-6-diamidino-2-phenylindole (DAPI; Sigma-Aldrich, Cat#: D9542) to label cell nuclei fluorescently and either 0.2 μl/ml phalloidin-iFluor 594 (Abcam, Cat#: ab176757) or phalloidin-iFluor 488 (Abcam, Cat#: ab176753) to label F-actin. Slides were rinsed and washed 3 × 5 min with PBST and cover slipped with Fluoromount G (Southern Biotech, Birmingham, AL).

For whole mount immunohistochemistry, the following arm slice explants were prepared: dissected axial nerve cord, 0.5 cm–1 cm transverse slices of arm, longitudinally bisected slices, and horizontally bisected slices. Explants were washed 3 × 15 min in PBST, dehydrated in a graded methanol series (25, 50, 75% in PBST, each for 10 min), rinsed twice in 100% methanol for 10 min, and stored overnight at −20 °C. The next day, explants were rehydrated in a graded methanol series (75%, 50%, 25% in PBST, each for 5 min) and rinsed twice in PBST for 5 min. Then, tissue was incubated for 60 min at 37 °C in a proteinase K solution (19.4 μg proteinase K per milliliter of PBST), post fixed for 15 min in 4% PFA/PBS, washed 3 × 15 min and 1 × 60 min in PBST, and blocked for an hour in 10% goat serum/PBST. Slices were then incubated in primary antibody for 7 days at 37 °C. Following primary incubation, tissue was rinsed 1x, 3 × 15 min, 5 × 60 min and overnight in PBST. Tissue was transferred to secondary antibody for seven days at 4 °C. Next, the tissue was rinsed with PBST 1x quickly, 3 × 15 min, 2 × 60 min, washed with DEPC-PBS 3 × 15 min, and post fixed for four days at 4 °C. Explants were then rinsed 3 × 15 min in PBS and cleared in a modified version of FRUIT (incubations in 35, 40, 60, 80, 100% FRUIT, each for 24 h)[62]. Slices were stored in 100% FRUIT at 4 °C until imaged.

Picrosirius Red

Collagen in squid and octopus samples was examined with Picrosirius Red (Abcam, Cat#: ab150681). Gelatin was melted off at 72 °C for 4–6 h before slides were dried and processed at room temperature. Slides were rinsed 3 times with deionized water, before being rehydrated for 1 min. Sections were incubated in Picrosirius Red for 5–10 min. Slides were de-stained with two rinses of acetic acid wash, before being dehydrated in 100% EtOH and mounted with Eukitt (Sigma Aldrich).

Hematoxylin and Eosin staining

Gelatin was melted off sectioned tissue at 72 °C for 4–6 h before slides were dried and processed at room temperature. Slides were rehydrated in deionized water and incubated in Mayer's Hematoxylin (HAE-IFU, ScyTek) for 1 min, before rapid rinsing in water to prevent overstaining. Tissue was briefly incubated in a bluing solution (HAE-IFU) for 15 seconds. The tissue was then dehydrated in an ethanol series (70%, 95% and 100%) before being moved into Eosin Y (HAE-IFU) for 1 min. Slides were rinsed in 100% EtOH, cleared in Histoclear (National Diagnostics, Atlanta, GA) for 1 min and mounted with Eukitt.

cDNA Synthesis and Cloning

Dissected octopus central brain tissue and arm tissue was flash-frozen on dry ice and stored at −80 °C until RNA extraction. Tissue was homogenized with a micropestle and RNA was extracted with Trizol Reagent (Invitrogen) and phasemaker tubes (Invitrogen) following manufacturer's instructions. RNA was stored at −80 °C in RNase-free water (Sigma-Aldrich) until used for cDNA synthesis with SuperScript III 1st-strand cDNA kit (Invitrogen) following manufacturer instructions. cDNA was diluted in RNase-free water and stored at −20 °C.

PCR primers were designed with MacVector software (version 12.6.0) or PrimerBlast from NCBI (Table 1). PCR reactions were conducted using the T100 thermocycler from BioRad. Reaction solutions were incubated at 95 °C for 5 min before undergoing 35–40 rounds of amplification cycles: 95 °C for 30 seconds, 52–57 °C for 45 seconds, and 72 °C for 1 min. A final elongation step was performed at 72 °C for 10 min. The sequence for *Dpe SYT1* was synthesized by Twist Bioscience (South San Francisco, CA; Table 2).

PCR products and Twist sequence were studied by gel electrophoresis to confirm that the sizes of products were as expected. PCR reactions were ligated into a pGEM T-Easy plasmid (Promega). Closed inserts were Sanger sequenced by the UChicago Comprehensive Cancer Center DNA Sequencing Facility. Plasmids were linearized by SacII (New England Biolabs, Cat#: 50812058) or SpeI (New England Biolabs, Cat#: 50811989) restriction enzyme digestion to generate antisense templates. Following phenol-chloroform extraction of the template, antisense digoxigenin (DIG)-labeled riboprobes (Sigma-Aldrich, Cat#: 11277073910) were transcribed with SP6 or T7 RNA polymerase (New England Biolabs). After transcription, the residual template was digested with RNase-free DNase I (Sigma-Aldrich) at 37 °C for 45 min. Riboprobes were ethanol-precipitated and stored in 100 μl of DEPC-H_2O at −20 °C until use.

In Situ Hybridization

Slides of sectioned tissue were equilibrated to room temperature and post-fixed in mailers for 15 min in 4% PFA/PBS, washed 3 × 15 min in

Table 1 | Transcripts amplified for in situ hybridization

Gene	NCBI Accession	Forward Primer	Reverse Primer
Obi SYT1 **(Synaptotagmin 1)**	XM_014919324.1	5′ CCT GGG ATG GAT ATG TCT GG -3'	5′ GTT CGG AAG TCC CAA TAC GA-3'
Obi CPLX1 **(Complexin 1)**	XM_014919099.1	5′ AAA ATG GCG GCA AGT GTA GG 3'	5′ AAA GAG GTG AGG GGT TGT GC 3'
Obi MNX **(Motor neuron and pancreas homeobox)**	XM_014912376.1	5′ TGC ATT TGG TCA GGG TCA GC-3'	5′ TTT AGG CAA ACA GTT CGC TGG -3'
Obi LHX3 **(LIM homeobox 3)**	XM_052978610.1	5′ GAA TTC GCC CTT CGA TTA CAA 3'	5′ ACA GCT AAG CGT TGA AAC AG 3'
Obi NKX6 **(NK6 homeobox)**	XM_014926771.2	5′ GTC ATA GTT GAT AAA GAC GGC AAA C 3'	5′ GTT CTT GTT TCT TTT TAG CTG ATG C 3'
Obi PIEZO **(Piezo type mechanosensitive ion channel component)**	XM_014926525.1	5′ CTG GCC AGG CTT TGT CAA TC 3'	5′ TCC ATT GGA TCT TCA TTA GTT G 3'
Obi DRGX **(Dorsal root ganglia homeobox)**	XM_014929620.1	5′ GGT TAT GGT GCA TGA TGG CG 3'	5′ GCA CGT ACG GTC ATT TCT GC 3'

DEPC-PBS and incubated at 37 °C for 15 min in proteinase K solution (Sigma-Aldrich; 1.45 µg proteinase K per milliliter of 100 mM Tris-HCl [pH 8.0], 50 mM EDTA [pH 8.0]). Slides were post-fixed for 15 min in 4% PFA/PBS, washed 3 × 15 min in DEPC-PBS, and acclimated to 72 °C for one hour in hybridization solution (50% formamide, 5x SSC, 1% SDS, 200 µg/ml heparin, 500 µg /ml yeast RNA). Slides were transferred to mailers with 1–2 mg antisense riboprobe in 15 mL hybridization solution and incubated overnight at 72 °C. The next day, slides were treated 3 × 45 min in preheated Solution X (50% formamide, 5x SSC, 1% SDS) at 72 °C. Slides were washed 3 × 15 min in room temperature TBST (Tris-buffered saline with 1% Tween 20) and blocked at room temperature for one hour in 10% DIG buffer (Roche) in TBST.

Anti-DIG Fab fragments conjugated to alkaline phosphatase (Sigma-Aldrich, Cat#: 11093274910) were preabsorbed with octopus embryo powder in 1% DIG buffer in TBST for at least one hour. Slides were then incubated on a rocker overnight at 4 °C in preabsorbed antibody diluted to a final concentration of 1:5000 in 10% DIG buffer in TBST.

The next day, slides were rinsed once, washed 3 × 15 min, then 2 × 1 h in TBST. Slides were washed for 10 min in freshly prepared NTMT (100 mM Tris-HCl [pH 9.5], 100 mM NaCl, 50 mM MgCl2, 1% Tween 20). For the color reaction, slides were incubated in nitro blue tetrazolium (NBT, 100 mg/mL in 70% dimethyl formamide/30% DEPC-H20, Gold Biotechnology, St. Louis, MO) and 5-bromo-4-chloro-3-indolyl phosphate (BCIP, 50 mg/mL in 100% dimethyl formamide, Gold Biotechnology, St. Louis, MO) in NTMT. Color development proceeded at room temperature and was monitored for a maximum of 5 days. When reaction was complete, slides were washed in TBST overnight and dehydrated through a series of ethanol washes into Histoclear, and coverslipped with Eukitt (Sigma-Aldrich).

Tracing

Adult *O. bimaculoides* ($n = 13$) were anesthetized in 2% EtOH/ASW, and the distal portion of a single arm was amputated with a razor blade. The amputated arm was placed in ASW, and the animal was either returned to a bucket of ASW to recover or euthanized in 4% EtOH/ASW and perfused.

The amputated arm was cut into 0.5cm-1cm slices. Each slice ($n = 83$) was injected with CF® 488 A Dye Dextran (Biotium, Cat#: 80110; 2% solution, 10kD) using a 25 or 32 gauge Hamilton Syringe (Hamilton, model#: 7000.5), rinsed in filtered seawater, and incubated at room temperature in 221 media with NuSerum (36% Leibovitz L15-Media, 36% filtered seawater, 18% deionized water, 1% pen-strep, 10% NuSerum). After three hours, the slices were rinsed with filtered seawater and fixed in 4% PFA/PBS. Slices were prepared for gelatin embedding and sectioning as described above, sectioned at 50um, and counterstained with phalloidin-iFluor 594 (0.2 µl/ml in 1%PBST) and DAPI (0.01 mg/ml in 1% PBST) before imaging.

DiI Labeling

DiI crystals (Biotium, Cat#: 60016) were placed at various targets in 0.5–1 cm transverse and longitudinally bisected fixed arm explants. Slices were incubated in 1% PFA/PBS in the dark for 7–14 days. Following DEPC-PBS washes for 3 × 15 min, explants were cleared in a modified version of FRUIT (incubations in 35, 40, 60, 80, 100% FRUIT, each for 24 h)[62].

Vasculature Injections

Lab-raised 6-week-old *O. bimaculoides* ($n = 5$) were anesthetized in 2% EtOH/ASW. A small incision was made above the right orbital socket to provide access for the pulled glass electrode to enter the white body. Using a picopump, 3–5 µL of a heavy-weight dextran (Invitrogen, Cat#D1818, 70,000 MW, lysine fixable) was injected into each juvenile octopus and allowed to circulate throughout the body for 5 min. Animals were then transferred to a 4% EtOH/ASW for five minutes before immersion fixation in 4% PFA/PBS overnight at 4 °C. Injected animals were stored in PBS at 4 °C before further processing for imaging or immunostaining.

Imaging

The immunolabeled and tracing tissue was studied with a Zeiss Axioskop 50 upright microscope and a Leica MZ FLIII stereomicroscope, both outfitted with the Zeiss AxioCam digital camera and AxioVision 4.5 software system. Selected sections were also studied on a Leica SP5 Tandem Scanner Spectral 2-photon confocal microscope (Leica Microsystems, Inc., Buffalo Grove, IL) or scanned with an Olympus VS200 Research Slide Scanner (Olympus / Evident, Center Valley, PA) with a Hamamatsu ORca-Fusion camera (Hamamatsu Photonics, Skokie, IL). Whole mounts were imaged on a LaVision BioTec UltraMicroscope II (Miltenyi Biotec, Bergish Gladbach, Germany) run by ImSpector Pro v. 7_124 software (LaVision BioTec, Bielefeld, Germany). Collected images were corrected for contrast and brightness and false colored in FIJI (version 2.1.0/1.53c; National Institutes of Health (NIH)). Whole mount reconstructions were visualized with Arivis Vision4D software v. 3.1 (arivis AG, Rostok, Germany). Diagrams were drawn using GIMP v. 2.10.32.

Proximal-distal Analysis

To examine the segmentation pattern down the proximal-distal axis, two series were created: three evenly spaced arm explants from an arm on the right side of one animal sectioned longitudinally and stained with acTUBA, and three evenly spaced explants from an arm on the left side of a second animal sectioned longitudinally and stained with H&E. For cross sectional area, an arm explant was sectioned horizontally and stained with acTUBA. For segment counts on *D. pealeii*, counts were performed on sections of arm explant stained with ISH for *Dpe SYT1*.

https://doi.org/10.1038/s41467-024-55475-5

Table 2 | Sequence synthesized for in situ hybridization

Gene	NCBI Accession	Sequence Synthesized
Dpe SYT1 **(Synaptotagmin 1)**	D63797.1	AGGATGGCAAAAAGGGCTCAAAGGAGCTGTCGACCTCAAAGGTGTACAGTTACTGGGCAACTCTATCAAA- GAAAAGGTGCAGCCTGACTTGGAGGAACTGCCAATGAATATGGAAGACAATGAGGATGCAGAAAGTA- CAAAATCCGAAGTAAAATTAGGGAAACTTCAATATTCTATGGACTACGATTTTCAGAAAGGCGAGCTAACAGTTAACGTGATA- CAGGCTGCCGACCTACCAGGGATGGATATGTCTGGGACATCTGACCCATATGTCAAAGTCTATCTAATGCCCGACAAAAGAA- GAAATTTGAGACAAAAGTCCATCGGAAAACACTCAACCCAGTATTTAACGAATCGTTCACTTTTAAGAACGTTCCCTATGCTGA- TATTACGGGTAAGACACTTGTGTTTGCGATCTATGATTTTGATCGCTTTTCGAAA- CACGACCAAATTGGTCAAGTCCAAGTGGCAATGAACTCGATAGATCTTGGATCGGTCATGGAAGAGTGGAGAGATCTAACTAGCCCGGA- TAATGATGCTGAGAAGGAGAACAAGCTGGGTGACATTTGTTTCTCATTGCGA- TATGTTCCGACTGCTGGCAAACTGACCGTTGTCATCCTTGAGGCTAAAAATCTAAAGAAAATGGATGTTGGTGGACTATCA- GATCCTTATGTAAAGATATCGTTGATGCTTAACGGCAAGAGAATTAAGAAGAAGAAAACCACTGTCAAGAAGTGCACACTGAATCCA- TACTATAATGAGTCATTCGCGTTTGAAGTCCCGTTCGAACAAATACA- GAAAGTATCCCTCTATGTCACGGTGGTCGACTACGATCGCATTGGGACCTCTGAACCAATCGGACGAACCTTCCTG

Segment Counts. The number of segments were counted along a length of six suckers on the anterior and posterior side of the ANC. The counts for the anterior and posterior sides were averaged together, then divided by six to determine segments/sucker.

Segment Width. Four segments across six suckers on both the anterior and posterior side of the ANC were selected for width measurements and were tagged with either the external side of the ANC (ExA) or the internal side of the ANC (InA) (Supplementary Fig. 7a, b). The width of each segment along the proximal-distal axis was measured manually using the line tool in FIJI. Measurements on the anterior and posterior side were averaged together to get averages for ExA and InA. Total averages were found by additionally averaging ExA and InA.

Sucker Width. For six suckers in each explant, the width of the acetabulum was measured manually at the widest point using the line tool in FIJI.

Cell Density. For each of the segments selected for the width measurements, a rectangle spanning the width of the segment was taken. The number of nuclei, visualized by DAPI, within the rectangle was counted using the analyze particle function in FIJI. The area of the rectangle was also found in FIJI. Density was calculated as the number of nuclei/area. Averages for ExA and InA pooled across both the anterior and posterior side of the ANC as for segment width calculations.

Cross Sectional Area. Across three suckers, three segments on ExA and three segments on InA were selected for cross sectional area measurements. Visibility of each segment across the oral to aboral extent of the ANC was ensured. The width, defined as the length in the proximal-distal axis, and height, defined as the length perpendicular to the proximal-distal axis, were manually measured in FIJI. Cross sectional area was calculated as width x height.

Nerve analysis

Large scale nerve analysis was done by segmenting whole mount tissue, immunostained for nerve markers, acTUBA and SMI-31. To examine brachial nerves, two whole mounts of slices stained with acTUBA and one slice whole mount stained with SMI-31 were imaged transversely. To examine the oral nerves, two whole mounts labeled for acTUBA were imaged, one transversely and one longitudinally, and one whole mount with SMI-31 was imaged transversely. Nerve fibers going to the sucker and to the brachial musculature were traced using Simple Neurite Tracer (SNT, v. 4.2.0) in FIJI[63]. For nerve fibers targeting the sucker, the major trunks were traced until they began majorly branching at the sphincter of the sucker. Other branching prior to the sphincter were also excluded. For the brachial nerves, all branch points were followed until they connected with a part of the peripheral nervous system or positive labeling became indistinguishable.

Oral nerve analysis. The traces for the oral nerves were tagged as corresponding to ExA or InA and the 3D spatial coordinates outlining the traces were found using the SNT API (Supplementary Fig. 7a, b, h)[63]. The coordinates of tips of the nerve were translated such that the center of all the tips was set as the origin. Subsequently, each tip coordinate was normalized such that the vector from the origin to the tip has a magnitude of 1, creating a circle. To determine percentage of the sucker covered, the angular extent of ExA and InA tips around the circle was computed and divided by 360°. The spatial distribution of tips corresponding to the ExS and the InS was visualized using Matplotlib (v. 3.7.3).

Aboral and central nerve analysis. The traces for the brachial nerves were segregated into the central nerves targeting the oral brachial

musculature and the aboral nerves targeting the aboral brachial musculature (Supplementary Fig. 4a). The branching pattern of the nerves were characterized using the SNT Sholl analysis with 10 µm spacing (Supplementary Fig. 4b)[64]. The profile was then fit with a 5-degree polynomial and normalized via min-max normalization, where the maximum was set to the radius associated with the longest nerve, the nerve that reaches the skin. The 3D spatial coordinates, root, and tips of the nerves were found using the SNT API[63]. The average trajectory of the nerve was computed by creating a vector from the root of the nerve to the center of the process (Supplementary Fig. 4c). The unit vector for each average trajectory was found and divided by the magnitude of the longest nerve. The distribution of the tips in the aboral-oral and proximal-distal plane was visualized using Matplotlib (Supplementary Fig. 5a). Relation to the septa was determined using the oral roots as additional markers and used to color code the nerves.

Statistics

Unless otherwise stated, data are mean +/- standard error of the mean (sem). Using MATLAB (2021b), a two-way ANOVA followed by Tukey's post hoc test was conducted to test for significance along the proximal-distal axis and between the ExS and InS. Data were considered significant if $p < 0.05$. Sample size was not statistically predetermined, and all data were validated by at least two markers and at least two animals.

Reporting summary

Further information on research design is available in the Nature Portfolio Reporting Summary linked to this article.

Data availability

Raw data for nerve fiber traces and measurements are available at https://github.com/olsoncs/Neuronal-Segmentation-Cephalopod-Arms (https://doi.org/10.5281/zenodo.14064124). Exemplar image stacks are available at https://doi.org/10.5281/zenodo.14064132. Source data are provided with this paper.

Code availability

Custom code used to analyze proximal-distal series and nerve fiber patterns is available at https://github.com/olsoncs/Neuronal-Segmentation-Cephalopod-Arms (https://doi.org/10.5281/zenodo.14064124).

References

1. Hochner, B., Zullo, L., Shomrat, T., Levy, G. & Nesher, N. Embodied mechanisms of motor control in the octopus. *Curr. Biol.* **33**, R1119–R1125 (2023).
2. Olson, C. S. & Ragsdale, C. W. Toward an understanding of octopus arm motor control. *Integr. Comp. Biol.* **63**, 1277–1284 (2023).
3. Kier, W. M. & Stella, M. P. The arrangement and function of octopus arm musculature and connective tissue. *J. Morphol.* **268**, 831–843 (2007).
4. Kennedy, E. B. L., Buresch, K. C., Boinapally, P. & Hanlon, R. T. Octopus arms exhibit exceptional flexibility. *Sci. Rep.* **10**, 20872 (2020).
5. Grasso, F. W. Octopus sucker-arm coordination in grasping and manipulation. *Am. Malacol. Bull.* **24**, 13–23 (2008).
6. van Giesen, L., Kilian, P. B., Allard, C. A. H. & Bellono, N. W. Molecular basis of chemotactile sensation in octopus. *Cell* **183**, 594–604.e14 (2020).
7. Gutfreund, Y. et al. Organization of octopus arm movements: a model system for studying the control of flexible arms. *J. Neurosci.* **16**, 7297–7307 (1996).
8. Hanlon, R. T. & Messenger, J. B. *Cephalopod Behavior*. (Cambridge University Press, 2018).
9. Bidel, F., Bennett, N. C. & Wardill, T. J. *Octopus bimaculoides*' arm recruitment and use during visually evoked prey capture. *Curr. Biol.* **32**, 4727–4733.e3 (2022).
10. Young, J. Z. The number and sizes of nerve cells in *Octopus*. *Proc. Zool. Soc. Lond.* **140**, 229–254 (1963).
11. Young, J. Z. *The Anatomy of the Nervous System of* Octopus Vulgaris. (Claredon Press, Oxford, 1971).
12. Graziadei, P. The nervous system of the arms. in *The Anatomy of the Nervous System of* Octopus vulgaris 45–61 (Claredon Press, Oxford, 1971).
13. Richter, S. et al. Invertebrate neurophylogeny: suggested terms and definitions for a neuroanatomical glossary. *Front. Zool.* **7**, 29 (2010).
14. Rossi, F. & Graziadei, P. Nouvelles recherches sur le systeme nerveux du bras des cephalopodes avec des methodes specifiques pour le tissu nerveux. *Acta Anat. (Basel)* **22**, 202–215 (1954).
15. Nixon, M. & Young, J. Z. *The Brains and Lives of Cephalopods*. (Oxford University Press, 2003).
16. Nödl, M.-T., Kerbl, A., Walzl, M. G., Müller, G. B. & De Couet, H. G. The cephalopod arm crown: appendage formation and differentiation in the Hawaiian bobtail squid Euprymna scolopes. *Front. Zool.* **13**, 44 (2016).
17. Zullo, L., Eichenstein, H., Maiole, F. & Hochner, B. Motor control pathways in the nervous system of Octopus vulgaris arm. *J. Comp. Physiol. A* **205**, 271–279 (2019).
18. Rowell, C. H. Excitatory and inhibitory pathways in the arm of *Octopus*. *J. Exp. Biol.* **40**, 257–270 (1963).
19. Wollesen, T., Loesel, R. & Wanninger, A. Pygmy squids and giant brains: Mapping the complex cephalopod CNS by phalloidin staining of vibratome sections and whole-mount preparations. *J. Neurosci. Methods* **179**, 63–67 (2009).
20. Campos-Ortega, J. A. & Hartenstein, V. *The Embryonic Development of Drosophila Melanogaster*. (Springer Berlin Heidelberg, Berlin, Heidelberg, 1997).
21. Hubaud, A. & Pourquié, O. Signalling dynamics in vertebrate segmentation. *Nat. Rev. Mol. Cell Biol.* **15**, 709–721 (2014).
22. Clark, E., Peel, A. D. & Akam, M. Arthropod segmentation. *Development* **146**, dev170480 (2019).
23. Gutfreund, Y., Matzner, H., Flash, T. & Hochner, B. Patterns of motor activity in the isolated nerve cord of the octopus arm. *Biol. Bull.* **211**, 212–222 (2006).
24. Rowell, C. H. F. Activity of interneurones in the arm of the *Octopus* in response to tactile stimulation. *J. Exp. Biol.* **44**, 589–605 (1966).
25. Rossi, F. & Graziadei, P. Nouvelles contributions à la connaissance du système nerveux du tentacule des céphalopodes IV. Le patrimoine nerveux de la ventouse de *l'Octopus vulgaris*. *Acta Anat. Suppl.* **32**, 1–79 (1958).
26. Jessell, T. M. Neuronal specification in the spinal cord: inductive signals and transcriptional codes. *Nat. Rev. Genet.* **1**, 20–29 (2000).
27. Lumsden, A. & Keynes, R. Segmental patterns of neuronal development in the chick hindbrain. *Nature* **337**, 424–428 (1989).
28. Albertin, C. B. et al. Genome and transcriptome mechanisms driving cephalopod evolution. *Nat. Commun.* **13**, 2427 (2022).
29. Kier, W. M. & Smith, K. K. Tongues, tentacles and trunks: the biomechanics of movement in muscular-hydrostats. *Zool. J. Linn. Soc.* **83**, 307–324 (1985).
30. Kier, W. M. The musculature of coleoid cephalopod arms and tentacles. *Front. Cell Dev. Biol.* **4**, 10 (2016).
31. Kier, W. M. The musculature of squid arms and tentacles: ultrastructural evidence for functional differences. *J. Morphol.* **185**, 223–239 (1985).
32. Yekutieli, Y. et al. Dynamic model of the octopus arm. i. biomechanics of the octopus reaching movement. *J. Neurophysiol.* **94**, 1443–1458 (2005).

33. Kang, R. et al. Embodiment design of soft continuum robots. *Adv. Mech. Eng.* **8**, 168781401664330 (2016).
34. Laschi, C., Mazzolai, B. & Cianchetti, M. Soft robotics: technologies and systems pushing the boundaries of robot abilities. *Sci. Robot.* **1**, eaah3690 (2016).
35. Rus, D. & Tolley, M. T. Design, fabrication and control of soft robots. *Nature* **521**, 467–475 (2015).
36. Graziadei, P. Sensory receptor cells and related neurons in cephalopods. *Cold Spring Harb. Symp. Quant. Biol.* **30**, 45–57 (1965).
37. Graziadei, P. P. C. & Gagne, H. T. Sensory innervation in the rim of the octopus sucker. *J. Morphol.* **150**, 639–679 (1976).
38. Altman, J. Control of accept and reject reflexes in the octopus. *Nature* **229**, 204–206 (1971).
39. Sivitilli, D. M., Smith, J. R. & Gire, D. H. Lessons for robotics from the control architecture of the octopus. *Front. Robot. AI* **9**, 862391 (2022).
40. Kang, G. et al. Sensory specializations drive octopus and squid behaviour. *Nature* **616**, 378–383 (2023).
41. Wells, M. J. Tactile discrimination of surface curvature and shape by the octopus. *J. Exp. Biol.* **41**, 433–445 (1964).
42. Kim, S. S., Rouault, H., Druckmann, S. & Jayaraman, V. Ring attractor dynamics in the *Drosophila* central brain. *Science* **356**, 849–853 (2017).
43. Wang, T. et al. Neural Models and Algorithms for Sensorimotor Control of an Octopus Arm. Preprint at https://doi.org/10.48550/ARXIV.2402.01074 (2024).
44. Chipman, A. Becoming Segmented. in *Perspectives on Evolutionary Developmental Biology* (ed. Fusco, G.) 234–244 (Padova University Press, 2019).
45. Lemche, H. A new living deep-sea mollusc of the cambro-devonian class monoplacophora. *Nature* **179**, 413–416 (1957).
46. Vagvolgyi, J. On the origin of molluscs, the coelom, and coelomic segmentation. *Syst. Zool.* **16**, 153–168 (1967).
47. Kocot, K. M., Poustka, A. J., Stöger, I., Halanych, K. M. & Schrödl, M. New data from Monoplacophora and a carefully-curated dataset resolve molluscan relationships. *Sci. Rep.* **10**, 101 (2020).
48. Redl, E., Scherholz, M., Todt, C., Wollesen, T. & Wanninger, A. Development of the nervous system in Solenogastres (Mollusca) reveals putative ancestral spiralian features. *EvoDevo* **5**, 48 (2014).
49. Wilson, N. G., Rouse, G. W. & Giribet, G. Assessing the molluscan hypothesis Serialia (Monoplacophora+Polyplacophora) using novel molecular data. *Mol. Phylogenet. Evol.* **54**, 187–193 (2010).
50. Wanninger, A. & Wollesen, T. The evolution of molluscs. *Biol. Rev.* **94**, 102–115 (2019).
51. Clark, R. B. *Dynamics in Metazoan Evolution: The Origin of the Coelom and Segments*. (Claredon Press, Oxford, 1964).
52. Lopes, V. M. et al. Cephalopod biology and care, a COST FA1301 (CephsInAction) training school: anaesthesia and scientific procedures. *Invert. Neurosci.* **17**, 8 (2017).
53. Fiorito, G. et al. Guidelines for the care and welfare of cephalopods in research –a consensus based on an initiative by CephRes, FELASA and the Boyd Group. *Lab. Anim.* **49**, 1–90 (2015).
54. Piperno, G. & Fuller, M. T. Monoclonal antibodies specific for an acetylated form of a-tubulin recognize the antigen in cilia and flagella from a variety of organisms. *J. Cell Biol.* **101**, 2085–2094 (1985).
55. Baratte, S. & Bonnaud, L. Evidence of early nervous differentiation and early catecholaminergic sensory system during *Sepia officinalis* embryogenesis. *J. Comp. Neurol.* **517**, 539–549 (2009).
56. Chitnis, A. & Kuwada, J. Axonogenesis in the brain of zebrafish embryos. *J. Neurosci.* **10**, 1892–1905 (1990).
57. LeDizet, M. & Piperno, G. Detection of acetylated α-tubulin by specific antibodies. in *Methods in Enzymology* vol. 196 264–274 (Elsevier, 1991).
58. Shigeno, S. & Yamamoto, M. Organization of the nervous system in the pygmy cuttlefish, *Idiosepius paradoxus* ortmann (Idiosepiidae, cephalopoda). *J. Morphol.* **254**, 65–80 (2002).
59. Sternberger, N. H. & Sternberger, L. A. Neurotypy: the heterogeneity of brain proteins. *Ann. N. Y. Acad. Sci.* **420**, 90–99 (1983).
60. Grant, P., Tseng, D., Gould, R. M., Gainer, H. & Pant, H. C. Expression of neurofilament proteins during development of the nervous system in the squid *Loligo pealei*. *J. Comp. Neurol.* **356**, 311–326 (1995).
61. Grant, P. & Pant, H. C. *Compartment-Specific Phosphorylation of Squid Neurofilaments*. in *Methods in Enzymology* vol. 568 615–633 (Elsevier, 2016).
62. Hou, B. et al. Scalable and DiI-compatible optical clearance of the mammalian brain. *Front. Neuroanat.* **9**, 19 (2015).
63. Arshadi, C., Günther, U., Eddison, M., Harrington, K. I. S. & Ferreira, T. A. SNT: a unifying toolbox for quantification of neuronal anatomy. *Nat. Methods* **18**, 374–377 (2021).
64. Ferreira, T. A. et al. Neuronal morphometry directly from bitmap images. *Nat. Methods* **11**, 982–984 (2014).

Acknowledgements

We thank Dr. Chuck Winkler of Aquatic Research Consultants for providing us with octopuses and Drs. Caroline Albertin and Thea Rogers for the *D. pealeii* samples. Imaging was performed at the University of Chicago Integrated Light Microscopy Core (RRID: SCR_019197). We extend special thanks to Dr. Christine Labno and Mr. Khalil Rodriguez for their invaluable assistance. We also thank Ms. Caroline Miller for assistance with whole mount image processing, Ms. Amelia Cheng and Mr. Jan Kasal for assistance with tracer injections and tissue processing, and Ms. Aashna Moorjani for comments. This work was supported by the NIH Developmental Biology Training Program (HD055164, NGS) and the NSF GRFP (DGE-1746045, NGS), and by the NIH UF1NS115817 award (CWR).

Author contributions

The initial finding was made by C.S.O. and N.G.S. The project was designed by C.S.O. and C.W.R. N.G.S. and C.S.O. cloned the cDNA, and C.S.O. performed the in situ hybridization experiments. C.S.O. carried out the immunohistochemistry, H&E staining, neural tracing, and squid experiments. N.G.S. did the vascular injections and Picrosirius Red staining. C.S.O. imaged and traced the whole mounts. C.S.O. wrote the code and conducted the analyzes. C.W.R. supervised. C.S.O. wrote the manuscript with edits from C.W.R. and N.G.S.

Competing interests

The authors report no competing interests.

Additional information

Supplementary information The online version contains supplementary material available at https://doi.org/10.1038/s41467-024-55475-5.

Correspondence and requests for materials should be addressed to Cassady S. Olson.

Peer review information *Nature Communications* thanks Alexandra Kerbl and the other, anonymous, reviewers for their contribution to the peer review of this work. A peer review file is available.